



**HAL**  
open science

## Preparation and characterization of perfluorocarbon microbubbles using Shirasu Porous Glass (SPG) membranes

Romain Melich, Jean Pierre Valour, Sébastien Urbaniak, Frédéric Padilla, Catherine Charcosset

► **To cite this version:**

Romain Melich, Jean Pierre Valour, Sébastien Urbaniak, Frédéric Padilla, Catherine Charcosset. Preparation and characterization of perfluorocarbon microbubbles using Shirasu Porous Glass (SPG) membranes. *Colloids and Surfaces A: Physicochemical and Engineering Aspects*, 2019, 560, pp.233-243. 10.1016/j.colsurfa.2018.09.058 . hal-03033316

**HAL Id: hal-03033316**

**<https://cnrs.hal.science/hal-03033316v1>**

Submitted on 9 Dec 2020

**HAL** is a multi-disciplinary open access archive for the deposit and dissemination of scientific research documents, whether they are published or not. The documents may come from teaching and research institutions in France or abroad, or from public or private research centers.

L'archive ouverte pluridisciplinaire **HAL**, est destinée au dépôt et à la diffusion de documents scientifiques de niveau recherche, publiés ou non, émanant des établissements d'enseignement et de recherche français ou étrangers, des laboratoires publics ou privés.

# Preparation and characterization of perfluorocarbon microbubbles using Shirasu Porous Glass (SPG) membranes

Romain Melich<sup>a,b</sup>, Jean-Pierre Valour<sup>a</sup>, Sébastien Urbaniak<sup>a</sup>, Frédéric Padilla<sup>b,c,d</sup>, Catherine Charcosset<sup>a,\*</sup>

<sup>a</sup>Univ Lyon, Université Claude Bernard Lyon 1, CNRS, LAGEP UMR 5007, 43 boulevard du 11 novembre 1918, F-69100, VILLEURBANNE, France

<sup>b</sup>LabTAU, INSERM, Centre Léon Bérard, Université Lyon 1, Univ-Lyon, F-69003, LYON, France

<sup>c</sup>Department of Radiation Oncology, University of Virginia School of Medicine, Charlottesville, VA, USA

<sup>d</sup>Focused Ultrasound Foundation, 1230 Cedars Court, Suite 206, Charlottesville, VA, USA

---

## Abstract

Microbubbles are increasingly used in several fields, such as medical imaging for enhanced contrast ultrasound imaging. These microbubbles usually consist of a gas core stabilized by surfactants molecules. In this study, a technique using Shirasu Porous Glass (SPG) membranes was used to produce perfluorocarbon microbubbles. The microbubbles obtained were characterized by their size, size distribution, and stability. The effect of several parameters on the microbubble's size was investigated related to the process (transmembrane pressure,  $\Delta P$ , bubble point pressure,  $P_{BP}$ , shear stress,  $\tau_w$ ), membrane pore size,  $D_p$ , and formulation (gas, surfactants in the aqueous phase). The transmembrane pressure nor the shear stress ( $\tau_w$ ) had influence on the microbubble's size or size distribution for  $\Delta P/P_{BP} < 1.5$ . The decrease of the membrane pore size from 1.1, 0.5, to 0.2  $\mu\text{m}$  led to lower microbubble size 13.3, 6.36, and 4.42  $\mu\text{m}$ , respectively, which was associated with higher size distribution 16%, 24% and 31%, respectively due to the higher Laplace pressure exerted on smaller microbubbles leading to their destabilization. With the 1.1  $\mu\text{m}$  pore size membrane, perfluorocarbon microbubbles were obtained with a diameter of 13.3  $\mu\text{m}$  and coefficient of variation (CV) of 16% when stabilized by sodium dodecyl sulfate (SDS), 15.6  $\mu\text{m}$  with CV% of 23% when stabilized by Tween20, and 16.5  $\mu\text{m}$  with CV% of 26% when stabilized by Polyoxyethylene (40) stearate (PEG40S). These low CV were indication of monodispersity. Perfluorocarbon microbubbles had a smaller size than air microbubbles due to the lower surface tension that decreased the retention force, keeping the microbubbles at the pore opening. The stability study showed that the perfluorocarbon gas greatly increased the lifetime of the microbubbles with a slight increase in size of 1.3 after 90 s compared to 2.2 for air microbubbles. Overall, the membrane technique proved to be an effective, controlled and reproducible method to produce perfluorocarbon microbubbles at a high rate  $\sim 0.6 - 1.5 \times 10^{+10}$  microbubbles/min. The key factor that determines the microbubbles formation is the adsorption kinetics of the surfactant at the new gas-liquid interface at the pore opening.

*Keywords:* Microbubble, Shirasu Porous Glass membrane, Membrane emulsification, Perfluorocarbon gas

---

\*Corresponding author. Address: Univ Lyon, Université Claude Bernard Lyon 1, CNRS, LAGEP UMR 5007, 43 boulevard du 11 novembre 1918, F-69100, VILLEURBANNE, France. Tel.: +33 4 72 43 18 34

Email address: [catherine.charcosset@univ-lyon1.fr](mailto:catherine.charcosset@univ-lyon1.fr) (Catherine Charcosset)

## 1. Introduction

Microbubbles have many potential applications in chemical and food industries, process engineering, water treatment, pharmaceutical and medicine. Due to their small size (typically around some microns), microbubbles have a very large gas-liquid interface area per unit volume. Microbubbles can thus increase the efficiency of gas-liquid contacting devices, such as bubble columns, chemical reactors and fermenters [1]. In chemical industries, many gas-liquid reactions are based on the dispersion of gas bubbles in a continuous liquid phase to improve both hydrodynamics and mass transfer [2]. In the food industry, the density and texture of products such gel and cream-based foods can be improved by monodisperse gas microbubbles in these materials [1]. In wastewater treatments, microbubble aeration can enhance ozone and oxygen gas-liquid mass transfer [3]. In biomedical applications, microbubbles of 1-10  $\mu\text{m}$  in diameter (sized to flow safely through a patients smallest capillaries) are used as ultrasound contrast agent for imaging, and are also studied for drug, gene and metabolic gas delivery [4, 5, 6, 7]. For these applications, monodispersity can be essential to improve echographic image quality [8], and also to limit Ostwald ripening effect by reducing effective Laplace pressure difference between polydisperse microbubbles, leading to better microbubble stability.

To design these gas-liquid contacting devices, the control of the size and size distribution of microbubbles generated is very important. To improve the manufacturing process, gases with reduced solubility in water, such as fluorocarbons can be used [9, 10, 11]. Perfluorocarbons gases reduce the osmotic pressure [12], allowing an increase in the microbubble stability [13, 14] and presenting a lower surface tension [15]. The shell composition is also a key determinant for microbubble's physical properties as well as their acoustic behavior and imaging time. The shell core serves to prevent gas escaping from the core and avoid microbubbles coalescence [16, 17]. While for biomedical applications, microbubbles are shelled with phospholipids or albumin [18], soluble surfactants are also advisable for the production of microbubbles with perfluorocarbon, as they are easy to implement due to a rapid adsorption at gas-liquid interface, such as mixture of sorbitan monostearate Span 60 and polyoxyethylene 40 stearate (PEG40S) in aqueous media to produce perfluorocarbon-filled microbubbles by sonication [19]. Other possible shell materials include proteins, and biocompatible polymers such as Pluronic F68 [20].

The main techniques used to generate microbubbles are mechanical agitation or sonication and microfluidic technologies [7, 21, 22, 23, 24]. In mechanical agitation, the hydrophobic gas is dispersed within an aqueous surfactant solution by disruption of the interface via high-shear mixing. Mechanical agitation is highly efficient at generating microbubbles at a high production rate, however the size distribution is highly polydisperse which requires further fractionation, for example by centrifugation [14], decantation [25] or flotation under gravity [11]. These methods are not ideally adapted for physicochemical investigations [10]. Microfluidic technologies include flow-focusing [26, 27, 28], T-junctions [29, 30] and electrodynamic atomization [31]. These techniques provide microbubbles with very low polydispersity by a precise control of their size, however, microbubbles are produced at a very low rate and microchannels tend to clog when preparing microbubbles smaller than 10  $\mu\text{m}$ . The microfluidic methods are time-consuming [22], which requires new microfluidic

strategies in order to improve the production yield.

A membrane technique is an alternative to generate monodisperse microbubbles. This method was first proposed by Kukizaki et al. [1, 32, 33, 34, 35]. With this technique, monodisperse microbubble are produced  
40 by pushing air through a Shirasu porous glass (SPG) membrane (Figure 1). Air microbubbles were formed at the pore outlets and detached from the membrane by the shear force exerted by the continuous phase containing surfactant(s) flowing along the surface. The size and size distribution of the microbubbles depended on several parameters related to the membrane pore size [34], surface wettability of the SPG membrane [1], symmetry/asymmetry [33], process parameters such as shear stress [32, 34], transmembrane pressure [34],  
45 and surfactants in the aqueous phase [35]. SPG membranes have also been used for microbubble aeration in a biofilm reactor for wastewater treatment [3]. Other membranes were used such as ceramic tubular membranes (PALL, France) to generate air or nitrogen microbubbles in aqueous or organic phase (water or heptane) for gas-liquid reactors [2]. Other advantages of using the membrane technique are low energy consumption, simplicity of design, easy scale-up, and reproducibility [36].

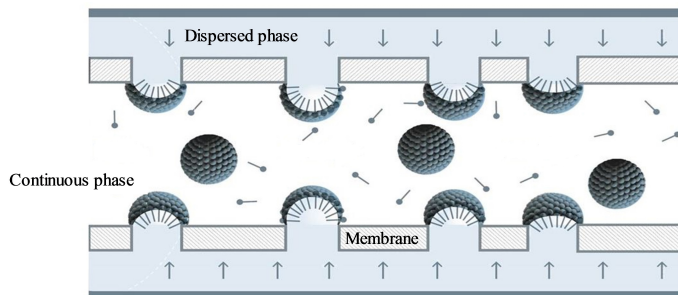


Figure 1: Schematic diagram of the membrane process principle where a gaseous phase is injected into the continuous phase composed of surfactants which stabilized the new interface

In this study, we considered the membrane technique to produce perfluorocarbon microbubbles. The  
50 microbubbles obtained with three different types of surfactants were characterized by their mean size and size distribution. The influence of the dispersed gaseous phase on microbubble formation was investigated. In addition, the microbubbles stability with each surfactant was observed. Surface tensions were also measured. The effect of several parameters on microbubbles characteristics were investigated such as shear stress, transmembrane pressure as well as surfactant types in the aqueous phase. In addition, perfluorocarbon mi-  
55 crobubbles produced by the membrane technique versus sonication were compared.

## 2. Materials and methods

### 2.1. Materials

The gas-liquid dispersion system was composed of perfluorocarbon or air as the dispersed gaseous phase  
60 and a continuous aqueous phase. Octafluoropropane ( $C_3F_8$ ) is a hydrophobic gas (vapor pressure of 792

kPa and water solubility at 25 °C of  $0.19 \text{ mol.m}^{-3}$  [37] purchased from F2 Chemicals Ltd (Preston, United Kingdom).

Three surfactants were used in this study: an anionic surfactant, sodium dodecyl sulfate (SDS), and two non-ionic surfactants, Polyoxyethylene (20) sorbitan monolaurate (Tween 20) and Polyoxyethylene (40) stearate (PEG40S) purchased from Sigma Aldrich (France). Ultrapure water was obtained using a Synergy unit system (Millipore, France) to prepare the aqueous solutions. The continuous phase was composed of 1.0 wt% surfactant in saline solution at 0.9% of NaCl for parenteral solution, since the microbubble preparation was found to be improved with the addition of NaCl [38]. Microbubble diameter was found to decrease when surfactant concentration increased, to achieve a minimum diameter for a concentration above the critical micelle concentration (CMC). Surfactants were therefore used at concentration above CMC to achieve maximum effect [39].

## 2.2. SPG membranes and membrane module

Hydrophilic tubular SPG membranes were provided by SPG Technology Co. Ltd (Miyazaki, Japan). The SPG membranes had a length of 125 mm and an inner diameter of 8.3 mm. These membranes are manufactured by a phase separation process of calcium aluminum borosilicate glass and subsequent acid leaching [32, 40], and have been widely used for production of emulsions and particles [41, 42]. Membrane with a mean pore size of 1.1, 0.8 and  $0.5 \mu\text{m}$  were used. The mean pore size data was provided by the manufacturer.

The microstructure of the membranes was observed by scanning electron microscopy (SEM) using a FEI Quanta 250 FEG microscope at the Centre Technologique des Microstructures at the University of Lyon (Villeurbanne, France). A fragment of SPG membrane was deposited on a flat steel holder. The sample was coated under vacuum by cathodic sputtering with copper. The samples were observed by SEM under an accelerating voltage of 10 kV. SPG membranes have cylindrical tortuous pores that form a three-dimensional network (figure 2). The membrane porosity is in the range of 0.53-0.60 [43]. SPG membranes are negatively charged and hydrophilic due to the presence of hydroxyl groups such as silanol groups on their surface. The dissociation of the silanol groups gives the negative charge of the SPG membrane surface [35].

## 2.3. Surface tension measurements

The surface tension of surfactant solutions was measured by the pendant drop method using a Drop Shape Analysis tensiometer model DSA-10 Mk2 (Krüss). A rising bubble (volume approximately of  $6 \mu\text{l}$ ) of air or  $\text{C}_3\text{F}_8$  was formed at the extremity of a needle using a syringe inside a quartz cell (10 ml) containing 1.0 wt% of surfactant solution at room temperature. The formation time of the bubble was about 1s. The system was calibrated using the outer diameter of the needle (outer diameter of 1.507 mm). The bubble was imaged with a CMOS camera, and its shape was then extracted by image analysis, and the surface tension,  $\gamma$ , was obtained as the best fit of the theoretical drop shape to the experimental profile [44].

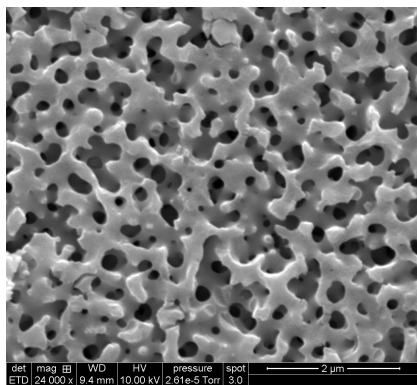


Figure 2: Scanning electron micrograph of the surface of the hydrophilic SPG membrane with a mean pore diameter of  $0.2 \mu\text{m}$

95 *2.4. Preparation of microbubbles*

*2.4.1. Probe-type sonication method*

Sonication is the most commonly used method for producing microbubbles which involves dispersing gas or liquid in a suspension of a suitable coating material using a high intensity ultrasound probe. The microbubble samples were prepared according to the method described by Ando et al. [20] by submitting a 1.0 wt% surfactant solution to brief sonication. The sonicator (Qsonica Q55 Sonicator, Newtown, USA) was equipped with a 3.2 mm probe and operated at 20 kHz. A surfactant solution of 6 ml was added to a 10 ml vial, and the atmosphere above the solution in the vial was filled with  $\text{C}_3\text{F}_8$  for 5 min. Then, microbubbles were formed by bringing the probe sonifier tip at around 5 mm below the gas-liquid interface of the solution and sonicating (amplitude 100%) for 15 s keeping a  $\text{C}_3\text{F}_8$  atmosphere above the solution.

105 *2.4.2. Membrane process using a cross-flow system*

The experimental set-up used for the microbubble formation experiments is shown in Figure 3. In this cross-flow system, the gas was used as the dispersed phase and a solution containing 1.0 wt% surfactant was used as the continuous phase and circulated to create a shear stress at the membrane surface to detach microbubbles. Before each experiments, the SPG membrane was placed in the beaker containing the continuous water phase and sonicated for 5 minutes to ensure complete membrane wettability. Indeed, Kukizaki et Wada [1] have reported the influence of the surface wettability on the microbubble formation, and only monodispersed microbubbles are created with a totally wet membrane characterized by a contact angle,  $\theta$ , smaller than  $45^\circ$ . The membrane was installed inside a cross-flow module of stainless steel supplied by SPG Technology. The effective length of the membrane was reduced to 105 mm due to sealing rings placed at both ends of the membrane tube. The new effective membrane area was then  $27.4 \text{ cm}^2$ . Then, the membrane module was placed horizontally and the continuous phase was circulated inside the membrane tube using a pump (Quattroflow 150S, Pall, France). Two conditions of shear stress were tested, corresponding to a fluid pressure of 0.73 Pa (with no rod inside the membrane) and 34.8 Pa (when a rod was inserted inside

the tubular membrane). The shear stress at the membrane wall,  $\tau_w$ , for a tubular membrane with a circular  
 120 section was calculated using the equation:

$$\tau_w = \frac{4\mu V_d}{R} \quad (1)$$

where  $R$  is the inner radius of the membrane tube (m),  $\mu$  is the dynamic viscosity (Pa.s) and  $V_d$  is the  
 mean velocity of the continuous phase in the tube ( $m.s^{-1}$ ).

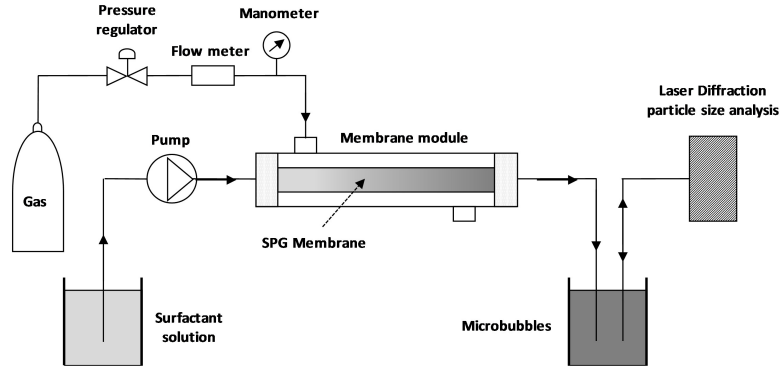


Figure 3: Experimental set-up to produce microbubbles using a tubular SPG membrane and to measure their size distribution  
 by laser diffraction particle size analysis

To obtain a high shear stress, a PTFE (polytetrafluorethylene) rod with a diameter of 6.35 mm was  
 introduced inside the tubular membrane. In this case, the shear stress at the membrane wall,  $\tau_w$ , was  
 125 calculated using the following equation:

$$\tau = 4\mu V_d \frac{R_2 - R_1}{R_1^2 + R_2^2 - \frac{R_2^2 - R_1^2}{\ln(R_2/R_1)}} \quad (2)$$

where  $R_1$  is the rod radius (m) and  $R_2$  is the inner membrane radius (m) [45]. Under these conditions,  
 the mean velocity of the aqueous phase was  $0.75 m.s^{-1}$  (with no rod inside the membrane) and  $5.18 m.s^{-1}$   
 when a rod was inserted inside the tubular membrane.

The gas was introduced on the external side and forced through the microporous membrane. At a pressure  
 130 higher than the bubble point pressure, the gas that passed through the membrane generated microbubbles  
 at the internal surface of the membrane. A pressure regulator (KPR1FRL412A20000, Swagelok), flowmeter  
 (Model SLA5850S, Brooks instrument) and manometer (PGI-63B-BG2.5-LASX, Swagelok) were added to  
 the set-up to control the gas pressure. The bubble point pressure was defined as the minimum transmembrane  
 pressure,  $\Delta P$ , needed to generate the first microbubbles appearing at the membrane surface. The bubble  
 135 point pressure,  $P_{BP}$ , can be estimated from Young-Laplace equation:

$$P_{BP} = \frac{4\gamma \cos\theta}{D_p} \quad (3)$$

where  $\gamma$  is the equilibrium surface tension at the gas-liquid interface,  $\theta$  is the contact angle, and  $D_p$  is the mean pore diameter. From this equation,  $P_{BP}$  can be estimated assuming that the contact angle is zero, due to the large number of hydroxyl groups on the membrane surface, which can be perfectly wetted by the aqueous phase [32]. The theoretical and measured bubble point pressures for the SPG membranes as  
 140 function of pore diameter are listed in Table 1. For all experiments, the transmembrane pressure applied was such that the ratio between transmembrane pressure and bubble point pressure,  $\Delta P/P_{BP}$ , was in the range of 1.1-1.5. The dispersed gas phase flux,  $J$ , was calculated from the volumic flowrate,  $Q$ , measured using the flowmeter:

$$J = \frac{Q}{A} \quad (4)$$

where  $A$  is the effective membrane area ( $27.4 \text{ cm}^2$ ).

## 145 2.5. Characterization of microbubbles

### 2.5.1. Laser diffraction measurement

The size and size distribution of microbubbles were measured using laser diffraction particle size analysis (Mastersizer 3000, Malvern Instrumentation, France) of a microbubbles sample diluted in a beaker of 500 ml under agitation at 1500 rpm. The technique is based on the measurement of the intensity of light scattered as  
 150 a laser beam passes through a dispersed particulate sample. The Mie-scattering theory was used to convert light scattering data to microbubble size distribution. The refractive index was 1.0 for the gas phase [46] and 1.33 for the continuous phase. The microbubble size measurement was the average of three successive laser diffraction runs. The results were expressed by  $D_{50}$ , the median diameter.

Two parameters were used to characterize the width of the size distribution, first the span of the mi-  
 155 crobubble size distribution, expressed as:

$$Span = \frac{D_{90} - D_{10}}{D_{50}} \quad (5)$$

where  $D_{90}$ ,  $D_{50}$  and  $D_{10}$  are the diameters corresponding to 90, 50, and 10 nb% on the relative cumulative microbubble size distribution curve, respectively. Then, the polydispersity was characterized by CV (coefficient variation) which is a measure of the standard deviation to  $D_{50}$  expressed in %, using the equation [22, 29, 47, 48]:

$$CV = \frac{\sum n_i |D_{50} - D_i|}{D_{50} \sum n_i} \times 100 \quad (6)$$

160 where  $D_i$ , is the mean diameter of the class  $i$  and  $n_i$  corresponds to the number of microbubbles of the class  $i$ .

To study stability, the microbubbles were collected at the membrane outlet and diluted into a beaker under agitation by a propeller to disperse homogeneously the MBs suspension. The microbubble suspension

was the circulated in the measurement cell of the Mastersizer instrument during 90 s and the size measured every 10 s.

### 2.5.2. Optical microscopy

Immediate observation and recording are important for accurately measuring the size and size distribution of microbubbles. After producing microbubbles, an aliquot of the dispersion was immediately diluted and added to a Malassez counting chamber (Marienfeld-Superior). The observations were carried out with a microscope (Leica DM LM, France). A CCD video camera (Leica MC120 HD) was connected to the microscope to capture images, which were visualized with Leica Application Suite (LAS EZ) software (Version 3.4.0).

## 3. Results and discussion

### 3.1. Comparison of sonication and membrane technique

Microbubbles were prepared by sonication and the membrane technique using a membrane with pore size of  $1.1 \mu\text{m}$ ,  $\Delta P/P_{BP} = 1.1$  and  $1.0 \text{ wt}\%$  SDS. The bubble size distributions are shown in figure 4. The microbubbles obtained had a mean size and span of  $D_{50}$ :  $13.3 \mu\text{m}$  and span:  $0.527$ ,  $D_{50}$ :  $14.3 \mu\text{m}$  and span:  $1.11$  using the membrane technique and sonication, respectively. The microbubble sizes were in the micrometric range size for both techniques, however, a narrower size distribution was obtained with the membrane than by sonication, which produced both smaller and larger bubbles. Figure 5 shows MBs obtained by the membrane technique and observed by optical microscopy just after their preparation.

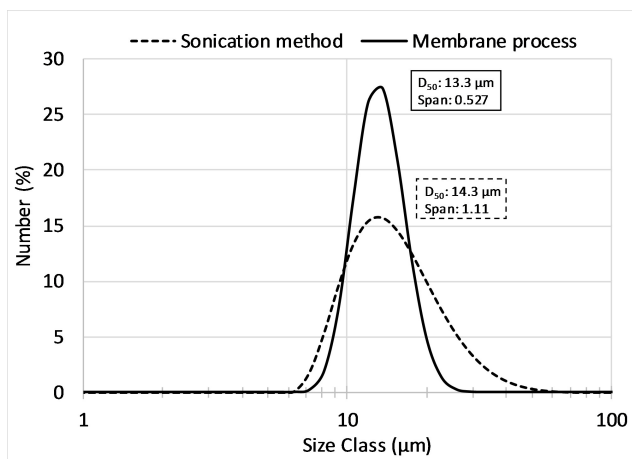


Figure 4: Comparison of the size of microbubbles generated by sonication and membrane with a mean pore diameter of  $1.1 \mu\text{m}$ . For both experiments, the continuous phase used was  $1.0 \text{ wt}\%$  SDS in water and the dispersed phase was  $C_3F_8$

Several techniques have also been compared by Stride [22] to produce microbubbles stabilized with L -  $\alpha$  - phosphatidylcholine, Tween 80 and Polyethyleneglycol (PEG) 40 stearate: sonication, coaxial electrohydrodynamic atomisation (CEHDA) and T-junction microfluidic. The CV% of microbubbles obtained were 150%, 38%, and 1%, for sonication, CEHDA and microfluidic, respectively. The CV% of microbubbles obtained

185 by the membrane technique was around 17% and therefore was between the one obtained with CEHDA and  
microfluidic device as reported by Stride [22].

Indeed, the membrane technique can produce microbubbles with a span close to the span of the SPG mem-  
brane pore size distribution, in the range of 0.4-0.6. A similar observation was reported for the preparation of  
emulsions with droplet size of several microns by Vladisavljević et al. [49]. Monodispersed microbubbles can  
190 be produced with a membrane of narrow pore size distribution. However, the microbubbles size distribution  
depends on several other parameters, like the aqueous phase composition. Without surfactant, large poly-  
disperse microbubbles were obtained due to microbubble coalescence at the pore opening by the membrane  
technique as shown by Kukizaki [35] or microchannel technique [48].

The yield of microbubbles obtained with the membrane was measured in the range  $0.6-1.5 \times 10^{+10}$  MBs/min  
195 while the one reported by microfluidic techniques was around  $2-6 \times 10^{+7}$  MBs/min. Our results are in agree-  
ment with previous studies reporting yields obtained by sonication [21].

Sonication has to be performed carefully in particular by considering the probe size compared to the  
vessel size, the position of the probe into the liquid, the frequency, the intensity and the time of sonication  
[11]. The membrane technique ( $\sim 10^{+8}$  MBs/s) may give a better reproducibility between different operators  
200 due to fewer parameters involved. These differences between these two techniques are due to the mechanisms  
involved in microbubble formation. Sonication involves using high intensity ultrasound to produce a suspen-  
sion of gas microbubbles in a liquid containing a suitable surfactant or polymer solution which adsorbs on the  
surfaces of the microbubbles to form a stabilizing coating. With the membrane technique, microbubbles are  
formed at the pore openings and can be detached by the continuous flowing aqueous phase. This technique  
205 involves much less energy, and the microbubbles size is controlled in part by the membrane pore size.

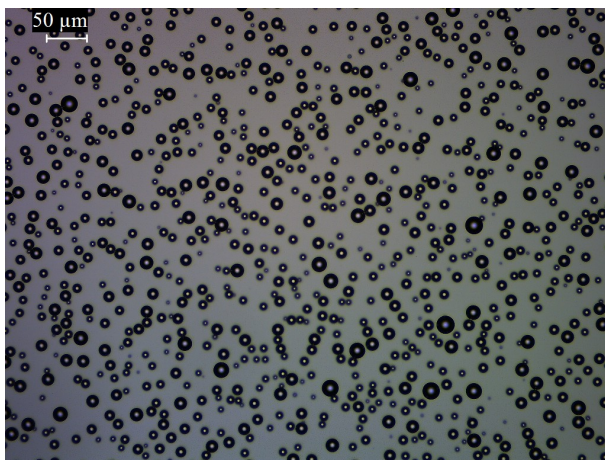


Figure 5: Immediate observation by optical microscopy of the size distribution of microbubbles generated by the membrane with a mean pore diameter of  $1.1 \mu\text{m}$ . The continuous phase used was 1.0 wt% SDS in water and the dispersed phase was  $C_3F_8$

### 3.2. Influence of process parameters

Microbubbles are formed in two steps, first microbubbles grow at the pore opening and then detach. The main forces that act on the microbubbles are the surface tension of the continuous phase, which is responsible for retaining the growing bubble at the pore opening, the static pressure difference force due to the pressure difference between the dispersed phase and the continuous phase at the membrane surface, and the drag force created by the continuous phase which detaches the microbubble from the membrane surface [42, 50]. The microbubble size is determined by the balance between these main forces. The surface tension force and the pressure difference force are opposite to each other.

During microbubble formation, the new interface created must be stabilized by surfactant molecules. Surfactants play two main roles: first, surfactant molecules adsorb at the new gas-liquid interface to reduce the surface tension and facilitate microbubble formation. Secondly, surfactants limit microbubble coalescence by stabilizing the newly created interface [50]. The adsorption kinetics of the surfactant at the gas-liquid interface is therefore a key factor which determines the microbubble size and size distribution [51]. To characterize the effect of the parameters that influence the microbubbles characteristics, we used SDS as the surfactant in the aqueous phase. This surfactant has a fast adsorption kinetics at the gas-liquid interface with a surface tension at  $t=0$  s,  $\gamma_0$ , equal to the surface tension at the equilibrium,  $\gamma_{eq}$ , (Table 1).

Surfactants	Gas	$\gamma_0$ ( $mN.m^{-1}$ )	$\gamma_{eq}$ ( $mN.m^{-1}$ )	$P_{BP}(Theo)$ (Bar)	$P_{BP}(Exp)$ (Bar)
SDS	Air	30.2	30.2	1.10	1.05
	$C_3F_8$	29.5	29.5	1.07	0.98
Tween 20	Air	42.0	37.5	1.36	1.35
	$C_3F_8$	40.2	36.1	1.31	1.25
PEG40S	Air	49.4	47.3	1.72	1.55
	$C_3F_8$	48.4	46.0	1.67	1.33

Table 1: Measured values of surface tensions,  $\gamma_0$ , at  $t=0$  s, and at the equilibrium,  $\gamma_{eq}$ , between gas-liquid interface for surfactant solutions, and the calculated  $P_{BP}(Theo)$  and the observed  $P_{BP}(Exp)$  values of pression of bubble point with a mean pore size of  $1.1 \mu m$  (theo: Theoretical and Exp: Experimental)

#### 3.2.1. Influence of the transmembrane pressure

For the three surfactants (SDS, Tween 20, and PEG40S) and the two gases (air and  $C_3F_8$ ),  $P_{BP}$  was calculated from the Young-Laplace equation (3) and the results are presented in Table 1. For all systems, the measured  $P_{BP}$  values were close to the calculated values which assumed the contact angle between the membrane and the aqueous continuous phase was equal to zero. This indicates that the membranes used in this study were wetted correctly by the continuous aqueous solution. However, we noted a larger difference between theoretical and experimental  $P_{BP}$  values for the two non-ionic surfactants (Tween 20 and PEG40S).

An electrostatic repulsive interaction exists between the anionic polar groups of the SDS molecules and the membrane surface (negatively charged). While for non-ionic surfactants, although no strong repulsion exists between the hydrophilic groups of the molecules and the membrane surface, a surfactant layer covers the hydrophilic groups of the membrane. It could be explained by a hydrophilic interaction between the hydrophilic groups of the surfactant and the surface maintaining the surfactant at the membrane. This interaction may affect the hydrophilicity of the membrane surface and thus the contact angle formed between the membrane surface and the water phase. This results in a higher contact angle value, and therefore to higher theoretical  $P_{BP}$  values than experimental ones. Experimental values were slightly lower than theoretical values, probably due the presence of larger pores than the mean pore size of  $1.1 \mu\text{m}$  which was used in the calculations. Indeed, a lower transmembrane pressure is needed to produce microbubbles through larger pores which is present due to the span pore size distribution around 0.4-0.6.

We studied the influence of transmembrane pressure on the perfluorocarbon microbubbles formation. For a concentration of 1.0 wt% SDS and with the  $1.1 \mu\text{m}$  pore size membrane, the variations of microbubbles size, size distribution and dispersed phase flux versus the ratio of  $\Delta P/P_{BP}$  are shown in Figure 6. At  $\Delta P/P_{BP} < 1$ , no microbubbles were observed. Perfluorocarbon monodispersed microbubbles were generated with the SPG membrane at transmembrane/bubble-point pressure ratio in the range of  $1 < \Delta P/P_{BP} < 1.5$ .

For a transmembrane/bubble point pressure ratio of  $\Delta P/P_{BP} < 1.5$ , the gaseous phase flux increased linearly with the ratio  $\Delta P/P_{BP}$ , while both mean microbubble size and size distribution were nearly constant (figure 6). This observed increase in gaseous phase influx is in agreement with Darcys law, which suggests that the dispersed phase flux increases proportionally to the transmembrane pressure. Microbubbles grow until they reach a certain size and then detach at the pore opening. At these low pressures, the surface tension force dominates other forces and the microbubble size and size distribution are independent of the transmembrane pressure.

For  $\Delta P/P_{BP} > 1.5$ , the flux, microbubbles size and size distribution increased sharply, indicating the formation of larger microbubbles with a broad size distribution. This result can be explained by the static pressure difference force which dominates at these higher pressures.

The range of pressure for which no effect on droplet characteristics was observed was called the "size-stable zone" [51]. The size-stable zone was already observed by Kukizaki et Goto [34] for air bubbles, for a ratio  $\Delta P/P_{BP} < 2$ . For the same surfactant used in our experiments, SDS, Kukizaki et Goto [34] found that the size-stable zone existed at higher pressure. This can be explained by the comparison of the difference in surface tension at the equilibrium. Indeed, the surface tension was  $36.5 \text{ mN.m}^{-1}$  in Kukizaki et Goto's article [34], while in our study, the surface tension was  $29.5 \text{ mN.m}^{-1}$  which implies a lower surface tension force for keeping the microbubble at the pore opening and a thus a faster microbubble detachment. This result was also reported by Kukizaki et al. [51] for droplets formed with two different concentrations of SDS, for which the lower interfacial tension presented a size-stable zone which ends at lower pressure.

The dispersed phase flux was  $1.28\text{-}2.55 \times 10^{-5} \text{ m}^3\text{m}^{-2}\text{s}^{-1}$  at  $\Delta P/P_{BP} < 1.5$  and for the  $1.1 \mu\text{m}$  for

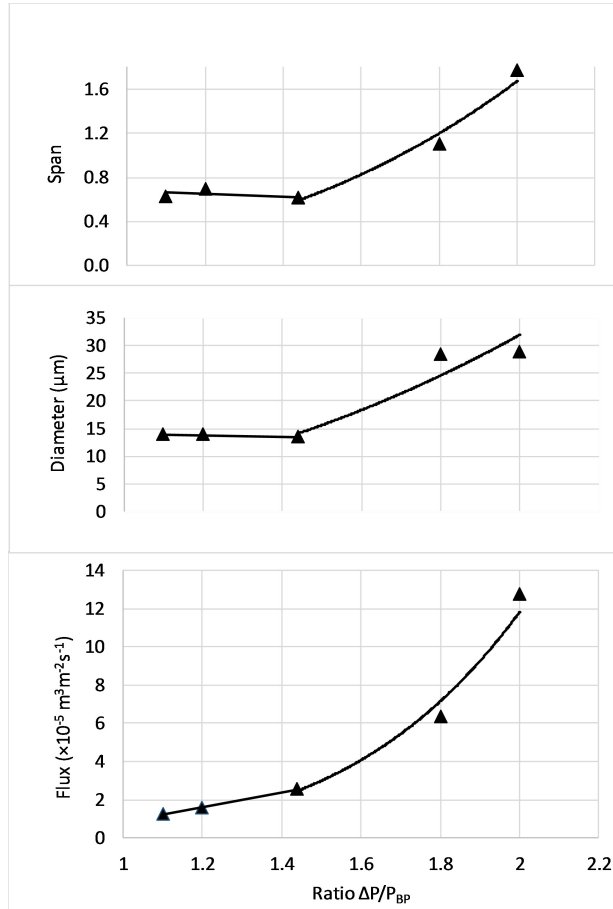


Figure 6: Influence of transmembrane/bubble point pressure ratio,  $\Delta P/P_{BP}$ , on the gaseous phase flux,  $J$ , microbubble diameter,  $D_{50}$ , and span of the distribution. Experimental conditions: gaseous phase was  $C_3F_8$ , mean pore of  $1.1 \mu\text{m}$ , with 1.0 wt% of SDS and a low shear stress

265 pore size membrane. These values are in agreement with the results of Kukizaki [33] who found  $6\text{-}15 \times 10^{-5} \text{ m}^3 \text{m}^{-2} \text{s}^{-1}$  for a symmetric SPG membrane with a size pore of  $1.58 \mu\text{m}$ . The authors also showed that the use of asymmetric SPG membranes significantly increased the air flux (around 40 times) when compared to symmetric SPG membranes. The use of asymmetric SPG membranes could be also an alternative to increase the production rate of perfluorocarbon microbubbles.

270 The  $\Delta P/P_{BP} = 1.1$  seems to be the best ratio to control the microbubble formation. Indeed, a ratio of 1 would be not necessary to activate a sufficient number of pores to obtain a great yield of microbubbles and a ratio around 1.4 or 1.5 produced a much higher gaseous flux which could lead to the loss of control of the microbubble formation.

### 3.2.2. Influence of the wall shear stress

275 The influence of shear stress of the continuous phase on microbubbles size and size distribution was measured for membranes with a mean pore size of  $1.1 \mu\text{m}$  and  $\Delta P/P_{BP}$ : 1.1 (Figure 7). Perfluorocarbon

microbubbles were prepared at two different shear stresses: 0.73 Pa (low shear stress) with a classical tubular module and 34.8 Pa (high shear stress) with an annular device. The low shear stress was used to recover the microbubbles at the membrane surface. With the 1.1  $\mu\text{m}$  pore size membrane, when increasing the wall shear stress from 0.73 to 34.8 Pa, the microbubble size distribution was the same at 13.3  $\mu\text{m}$  and 13.1  $\mu\text{m}$ , respectively. For both conditions, monodispersed microbubbles were produced with a CV% of 16% at low shear stress and 17% at high shear stress. However, we observed a better size repeatability at a high shear stress as shown by the error bars in Figure 7.

The influence of shear stress depends on other parameters like transmembrane pressure and interfacial tension. Vladisavljević [41] reported that two mechanisms of drop formation are possible: (1) a shear-controlled detachment as a result of shear stress on the membrane surface and (2) a spontaneous detachment driven by interfacial tension. For example, Kukizaki [33, 34] observed that when increasing the shear stress, the bubble size decreased to a limit value beyond which the size was independent of the applied shear stress. Generally, variation in size occurred at very low stress values and at high transmembrane pressures. When preparing emulsions, Vladisavljević et Schubert [43] showed that at high transmembrane pressures, the droplet size decreased when increasing the wall shear stress from 0.6 to 47 Pa, while at smaller transmembrane pressures, the size decreased very slightly, from 3.5 to 3.4  $\mu\text{m}$ , for wall shear stress of 0.55 Pa and 91 Pa, respectively.

In our study, the main principle to MBs formation at the tortuous and non-circular pores openings are driven by the second mechanism where the surface tension force dominates other forces (shear stress force, transmembrane pressure). In our case, the MBs size is independent on shear stress as we fixed a low transmembrane flux ( $\Delta P/P_{BP}$ : 1.1). The effect of the wall shear stress depends on the surface tension value. For example, Lepercq-Bost et al. [52] showed that at lower interfacial tension, the shear stress had a lower effect on the droplet diameter of emulsions generated by ceramic membranes. Indeed, at a lower surface tension, the force retaining the MBs or droplets at the pore opening is lower and the microbubble detachment is easier; this could explain the lower effect of shear stress on the droplet formation. In addition, our results show the same trend at a lower surface tension (1.0 wt% SDS ;  $\gamma$ : 29.5  $\text{mN}\cdot\text{m}^{-1}$ ) compared with the higher surface tension used by Kukizaki et Goto [34] (0.3 wt% SDS ;  $\gamma$ : 36.5  $\text{mN}\cdot\text{m}^{-1}$ ) who reported that the size was dependent on the shear stress. Indeed, the surfactant concentration influences considerably the surfactant adsorption kinetics and thus the dynamic surface tension [50]. At the higher surfactant concentration used in our study, the surface tension force dominated and the drag force created by the shear stress could not modify the microbubble size.

The mechanisms of microbubble production at low shear stress (0.73 Pa) may be compared to the ones suggested for spontaneous detachment of air MBs [32]. This detachment is governed by the surface tension at a low dispersed phase flux as explained above. The adsorption kinetics of surfactant from bulk to the new gas-liquid interface is a key parameter in the spontaneous detachment due to the absence of continuous phase flux. In this case, the tortuous pores and irregular cross-section of the SPG membrane (Figure 2) facilitates

the generation of the microbubbles. In addition, the dispersed phase deformation by the non-circular pores leads to the formation of a neck which may facilitate the MBs detachment, as observed for droplet production [53].

315

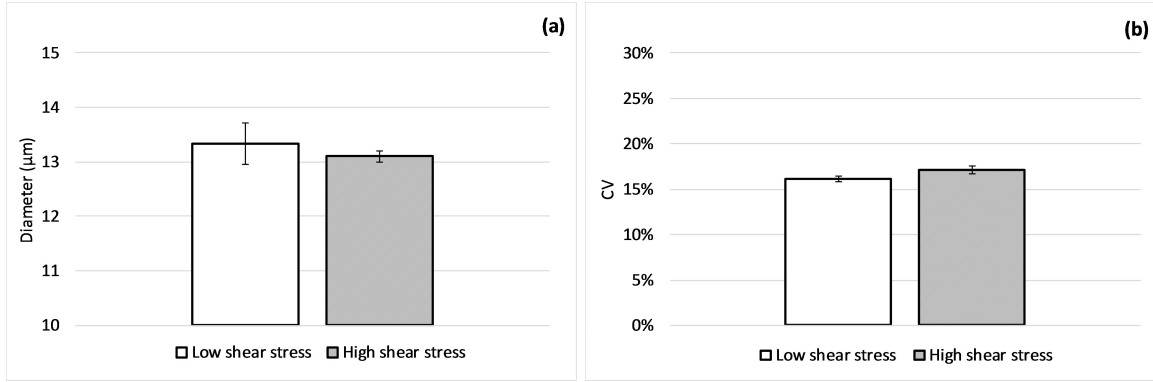


Figure 7: Influence of shear stress,  $\tau_w$ , (a) on the microbubble diameter and (b) on the CV% for membrane mean pore size 1.1  $\mu\text{m}$  at experimental conditions: continuous phase 1.0 wt% SDS in water, gaseous phase  $\text{C}_3\text{F}_8$ , and ratio  $\Delta P/P_{BP}$ : 1.1

### 3.2.3. Influence of the pore size

Perfluorocarbon microbubbles were prepared with the 0.2, 0.5 and 1.1  $\mu\text{m}$  pore size membranes. The three experiments were realized with a continuous phase containing 1.0 wt% SDS,  $\Delta P/P_{BP}$ : 1.1 and at a low shear stress (0.73 Pa). The mean diameter of the microbubbles obtained is shown in Figure 8. As expected, the microbubble mean size decreased when the membrane pore size was decreased. We observed a relationship between MBs size and pore size that seems exponential, but this would have to be confirmed with other pore size membranes. Other studies have reported linear relations with pore sizes in the range of 1 to 10  $\mu\text{m}$ , where the  $D_{MBs}/D_{Pore}$  ratio was between 7 and 10 depending of the surfactant used [33, 35]. In our study, we found a ratio of  $D_{MBs}/D_{Pore}$  around 12 for the 0.5 and 1.1  $\mu\text{m}$  pore size membranes, in agreement with a possible linear relationship. But for the smallest pore size used of 0.2  $\mu\text{m}$ , we found a ratio of 22. This result may be explained by an initial growth period due to the influx of air dissolved ( $\text{N}_2$  and  $\text{O}_2$ ) in water diffusing into the PFC MB [54]. Also the growth caused a decrease of the Laplace pressure, which is inversely proportional to the MBs radius. The Laplace pressure,  $\delta P$ , is the main mechanism which is responsible of the disappearance of a MB, given by the equation:

320

325

$$\delta P = \frac{2\gamma}{r} \quad (7)$$

330

where  $\gamma$  is the surface tension and  $r$  is the radius of the microbubble. The Laplace pressure is very high for microbubbles with small size. As a result, the microbubble size distribution changes over time, with the larger bubbles growing in size and the smaller microbubbles shrinking and then finally disappearing. This explains the polydisperse distribution, characterized by a coefficient of variation of 31%, of microbubbles obtained with the 0.2  $\mu\text{m}$  pore size.

335

For comparison, when preparing droplets by membrane emulsification, the  $D_{Droplets}/D_{Pore}$  ratio was found lower, in the range of 3.1-3.7 [43]. Indeed, the oil droplet diameter decreased when increasing the dispersed phase viscosity [51]. Therefore, for the same membrane, the oil droplets size is expected to be lower than the microbubbles size. This results in a  $D_{Droplets}/D_{Pore}$  ratio lower than the  $D_{MBs}/D_{Pore}$  ratio.

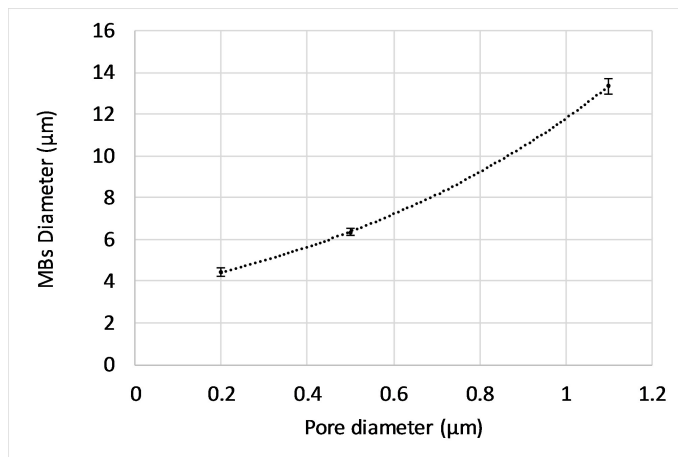


Figure 8: Influence of mean pore size (0.2, 0.5 and 1.1  $\mu\text{m}$ ) on the microbubble diameter,  $D_{50}$ , at experimental conditions: continuous phase 1.0 wt% SDS in water and ratio  $\Delta P/P_{BP}$ : 1.1

### 3.3. Influence of the surfactant type

340

Perfluorocarbon microbubbles were prepared with different surfactants: SDS, Tween 20, PEG40S in the continuous phase at 1.0 wt%. The 1.1  $\mu\text{m}$  pore size membrane was used, at a low shear stress (0.75  $\text{m.s}^{-1}$ ), and  $\Delta P/P_{BP}$ : 1.1. Uniform size distributions were obtained with the various surfactants as shown in Figure 9. The smallest size and narrower dispersity were obtained with SDS, followed by Tween 20 and PEG40S. These results can be related to the equilibrium and dynamic surface tension of the various solutions measured by the pendant drop method (Figure 10). The three surfactants showed different equilibrium surface tension, the lowest being obtained with SDS (29.5  $\text{mN.m}^{-1}$ ), then Tween 20 (36.1  $\text{mN.m}^{-1}$ ), and the highest with PEG40S (46.0  $\text{mN.m}^{-1}$ ). As explained previously, at a lower surface tension, the force retaining the microbubble at the pore opening is lower and the microbubble detachment is easier, resulting in microbubbles with smaller size and better monodispersity with SDS.

345

350

355

In addition, the three surfactants showed different adsorption kinetics, the fastest adsorption kinetics being obtained with SDS and the lowest with PEG40S. When a microbubble is formed, the equilibrium surface tension,  $\gamma_{eq}$ , of the surfactant solution is not reached instantaneously. The surfactant molecules must diffuse at the new interface from the bulk solution, their hydrophobic tails directed toward the gaseous phase. For a surfactant with a fast adsorption kinetic, such as SDS, the surface tension at  $t=0$  s is close to the equilibrium surface tension and the microbubbles detach faster from the membrane surface. This results in microbubbles with smaller size and better uniformity. Therefore, larger and more polydisperse microbubbles

were obtained with surfactants having the slowest kinetics (Tween 20 and PEG40S). This result was also observed for oil droplets produced by membrane emulsification, as reported by Schröder et al. [50]: the faster a surfactant adsorbs at the new interface, the smaller the droplets produced. In addition, surfactants with faster adsorption kinetics help to reduce the probability of microbubbles coalescing at the pore opening, which also results in microbubbles with smaller size and better monodispersity.

Another parameter that can influence coalescence is the interaction between the hydrophilic head groups of the surfactant and the membrane surface [35]. The surfactant molecules must not interact with the membrane surface by electrostatic interactions or Van der Waals forces, as this could result in a change of the membrane hydrophobicity. In the case of SDS, the presence of negative charges on the head groups of the SDS molecules and the membrane surface facilitates the microbubbles detachment by electrostatic repulsion and improves the size distribution compared to Tween 20 and PEG40S which do not present negative charges on their head groups. Overall, surfactants play an important role to produce monodisperse microbubbles by the membrane technique.

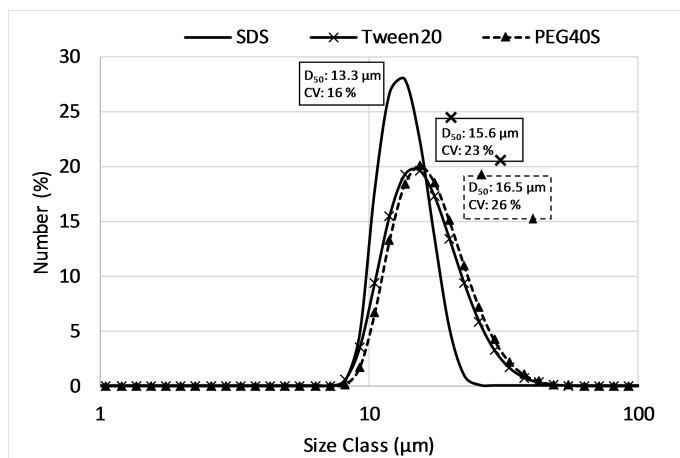


Figure 9: Influence of the surfactants at a concentration of 1.0 wt% on the microbubble size distribution. Experimental conditions: gaseous phase was  $C_3F_8$ , membrane mean pore size  $1.1 \mu\text{m}$  and ratio  $\Delta P/P_{BP}$ : 1.1

### 3.4. Influence of the gaseous phase

Figure 10 shows the dynamic surface tension of the bubbles as a function of time for the three surfactants at 1.0wt%. The decrease of the surface tension corresponds to the progressive adsorption of surfactant molecules at the gas-water interface until equilibrium. The initial surface tension value,  $\gamma_0$ , is around  $72 \text{ mN}\cdot\text{m}^{-1}$  at the air-water interface and  $70.1 \text{ mN}\cdot\text{m}^{-1}$  at the perfluorocarbon-water interface in the absence of surfactant. These values at  $t=0$  s were not measurable in presence of 1.0wt% surfactant due to rapid adsorption kinetics. The presence of perfluorocarbon in the microbubbles significantly decreased the interfacial tension at equilibrium,  $\gamma_{eq}$ , compared with air. A higher decrease of the surface tension at equilibrium was observed from  $37.5$  to  $36.1 \text{ mN}\cdot\text{m}^{-1}$  for Tween 20 and  $47.3$  to  $46.3 \text{ mN}\cdot\text{m}^{-1}$  for PEG40S after 4 min. For

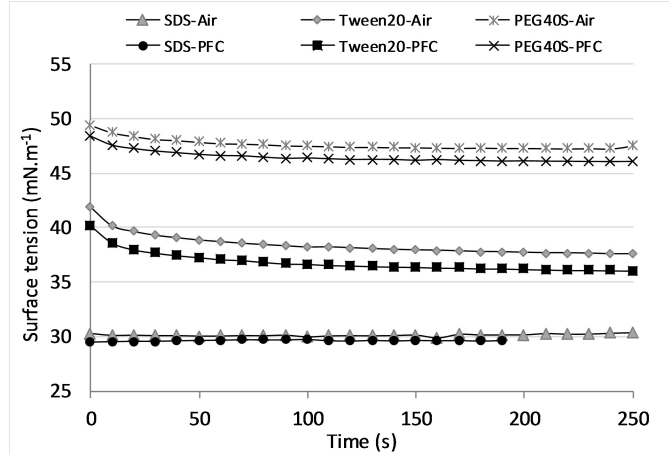


Figure 10: Surface tension at the gaseous/liquid interface for various surfactants at 1.0 wt% and air or  $C_3F_8$  at room temperature (PFC: Perfluorocarbon)

SDS, this effect was less pronounced due to the fast adsorption of the surfactant at the gas-liquid interface. As reported by Nguyen [15] for phospholipids, the perfluorocarbon gas increased the adsorption kinetic of the surfactant and decreased the equilibrium surface tension. These authors concluded that perfluorocarbon acts as a cosurfactant at the gas-liquid interface, despite the absence of any amphiphilic character.

As explained in the previous sections, a lower surface tension allows obtaining smaller microbubbles, by decreasing the retention force which keeps the microbubble at the pore opening and thus facilitating the microbubble detachment. Indeed, we observed a decrease of the microbubble size with the use of perfluorocarbon gas compared with air for three surfactants (Figure 11). The decrease of microbubble size was less pronounced with SDS than for the two other surfactants, due to a smaller decrease of the equilibrium surface tension.

### 3.5. Microbubbles stability

Stability of perfluorocarbon microbubbles stabilized by the three surfactants at 1.0 wt% was measured during 90 s. The perfluorocarbon microbubbles were prepared with the membrane of pore size  $1.1 \mu\text{m}$  and  $\Delta P/P_{BP}$ : 1.1 (Figure 12). Air microbubbles stabilized with SDS and prepared at the same experimental conditions were also tested. In all cases, the mean size of the microbubbles increased with time. This increase was less pronounced for perfluorocarbon microbubbles (1.2 for microbubbles stabilized with SDS between  $t=0$  s and  $t=90$  s) compared with air microbubbles (2.2 times size increase). For the three surfactants tested, the size of the perfluorocarbon microbubbles increased in a similar way, the increase being equal to 1.29 for Tween 20 and 1.33 for PEG40S. Figures 12 and 13 show two main trends: an increase in microbubble size associated to a decrease in microbubbles concentration. This is the result of the disappearance of the smaller microbubbles while the larger microbubbles grow in size.

The variation of microbubbles diameter over time presents two main stages: (1) an initial growth period,

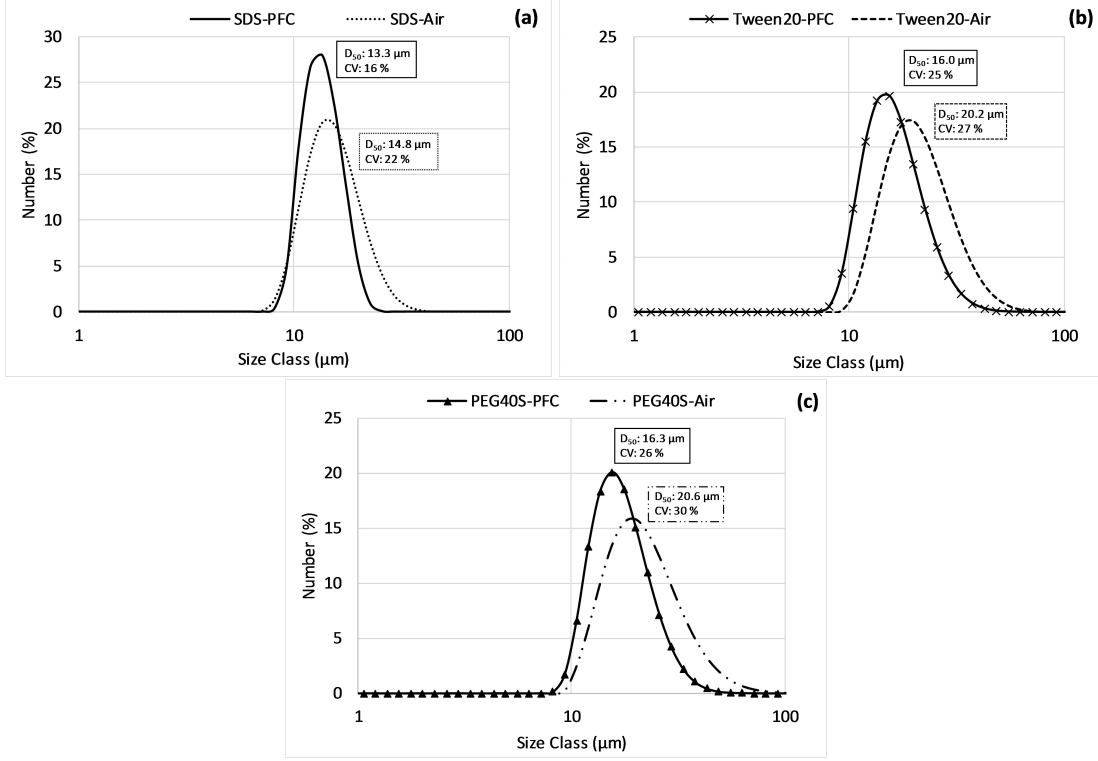


Figure 11: Influence of the gaseous phase on the microbubble size distribution stabilized with 1.0 wt% (a) SDS, (b) Tween 20 and (c) PEG40S. Experimental conditions: membrane mean pore size 1.1  $\mu\text{m}$  and ratio  $\Delta P/P_{BP}$ : 1.1 (PFC: Perfluorocarbon)

(2) followed by microbubble dissolution. The fast initial growth of the microbubble is due to the influx of air dissolved in water diffusing into the PFC microbubble [54]. The microbubble dissolution is mainly related to the Laplace pressure experienced by a gas microbubble, given by equation 7. As gas leaves the microbubble, due to the pressure gradient, the bubble shrinks and the Laplace pressure increases, which accelerates the rate of gas dissolution and the resulting bubble shrinkage. The surfactant at the gas/water interface reduces the gas/water surface tension and thus decreases the Laplace pressure, but does not eliminate it. The rate of bubble shrinkage as a function of time ( $t$ ) resulting from the dissolution of the gas into the bloodstream is predicted by the equation 8 [12, 55]:

$$\frac{dr}{dt} = -LD_w \left[ \frac{P^* + \frac{2\gamma}{r}}{P_{atm} + \frac{1}{3r}} \right] \left[ \frac{1}{r} + \frac{1}{\sqrt{D_w t \pi}} \right] \quad (8)$$

where  $L$  is the Ostwald coefficient,  $D_w$  is the gas diffusivity in water,  $\gamma$  is the surface tension,  $P_{atm}$  is the atmospheric pressure, and  $P^*$  is the excess pressure [12, 37]. Equation 8 predicts that the inclusion of perfluorocarbon gas with low solubility in water (which gives a low Ostwald coefficient) increases the lifetime of a microbubble. The Ostwald coefficient is defined as the partition coefficient of the gas between the gaseous phase and aqueous phase (ratio of the solubility of the gas in the liquid to the density of the gas).

The lower the Ostwald coefficient, the longer the lifetime of the microbubbles since perfluorocarbon gases  
 415 ( $L_{C_3F_8}$ :  $583 \times 10^6$ ;  $25^\circ\text{C}$ ) are less water-soluble than the air ( $L_{O_2}$ :  $31\,110 \times 10^6$  and  $L_{N_2}$ :  $15\,880 \times 10^6$ ;  $25^\circ\text{C}$ )[40]. The gas diffusion coefficient,  $D_w$ , is inversely proportional to the gas molecules size, which results in a decrease in diffusivity for  $C_3F_8$  ( $188\text{ g.mol}^{-1}$ ) compared to air ( $28.9\text{ g.mol}^{-1}$ ).

The concentration of perfluorocarbon microbubbles stabilized with SDS was constant during 60 s, before decreasing, while the air microbubbles concentration decreased from  $t=0$  s (Figure 13). The mechanism by  
 420 which larger microbubbles grow in size at the expense of smaller bubbles is called Ostwald ripening. The dissolution of the gas in the aqueous phase increases as the interfacial curvature increases and then the bubble size decreases quickly. Thus, perfluorocarbon microbubbles showed a better stability than air microbubbles.

Another phenomenon occurs at the gas-liquid interface, where the dynamic adsorption and desorption of the surfactant molecules creates short spaces between molecules, facilitating the gas transfer [56]. In the  
 425 case of perfluorocarbon microbubbles stabilized with PEG40S, the gas transfer into the aqueous phase could be increased, due to the low cohesive shell created by steric repulsion between the hydrophilic heads of the PEG40S macromolecules. This could explain the faster decrease of PEG40S perfluorocarbon microbubble concentration.

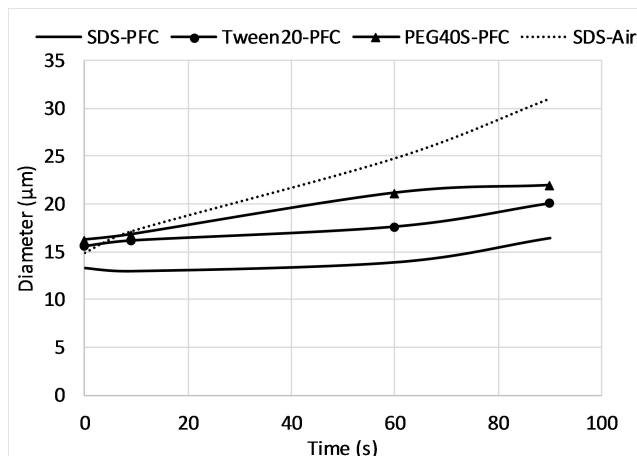


Figure 12: Variation of microbubble diameter,  $D_{50}$ , as a function of time for various surfactants with  $C_3F_8$  or air. Experimental conditions: membrane mean pore size  $1.1\ \mu\text{m}$  and ratio  $\Delta P/P_{BP}$ : 1.1 (PFC: Perfluorocarbon)

However, the lifetime of the microbubbles obtained with the surfactants was low compared with microbubbles  
 430 stabilized by lipids [14]. These microbubbles could then be used as transiently stable microbubbles as shown by Dhanaliwala et al. [27], as large microbubbles ( $19\ \mu\text{m}$ ) produced by microfluidic process were administered *in vivo* in a mouse and shown to generate a large acoustic response in both the right and left ventricles.

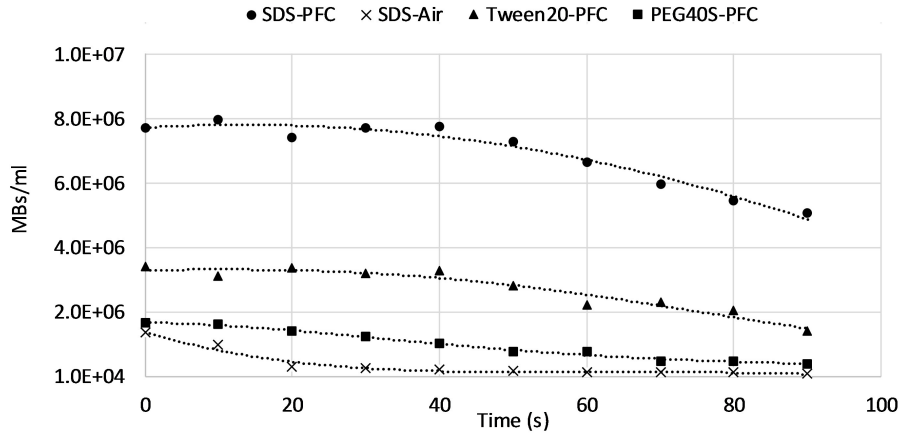


Figure 13: Variation of concentration MBs/ml as a function of time for various surfactants with  $C_3F_8$  or air. Experimental conditions: membrane mean pore size  $1.1 \mu\text{m}$  and ratio  $\Delta P/P_{BP}$ : 1.1 (PFC: Perfluorocarbon)

#### 4. Conclusion

435 In this study, we produced successfully perfluorocarbon microbubbles with the use of tubular SPG membranes with a  $1.1 \mu\text{m}$  pore size and  $\Delta P/P_{BP}$ : 1.1. The microbubbles were generated with a mean diameter of 13.3, 15.6 and  $16.5 \mu\text{m}$  with a narrow size distribution for the three surfactants SDS, Tween20 and PEG40S, respectively. The effect of transmembrane pressure, shear stress at the membrane surface due to the water phase flow, and pore size on the microbubbles size was investigated. The transmembrane pressure, until a  
440 threshold of  $\Delta P/P_{BP} < 1.5$ , and shear stress did not affect the size of the microbubbles which were produced at a high yield ( $\sim 10^{+10}$  MBs/min). As expected, the decrease of the pore size led to a decrease of the microbubble size, but the dilution of microbubbles into a beaker before the size measurement by laser diffraction increased their dissolution which impacted their size and size distribution. This study also showed that the perfluorocarbon gas decreased the surface tension at the gas-water interface to produce smaller microbubbles  
445 compared with air microbubbles and that the hydrophobicity properties of the perfluorocarbon gas increased the microbubbles stability. The main phenomenon governing the formation of monodispersed microbubbles by the membrane technique is the adsorption kinetics of the surfactant at the new gas-liquid interface at the pore opening.

## Nomenclature

A	Effective membrane area ( $m^2$ )
$D_i$	Mean diameter in the class i ( $\mu m$ )
$D_n$	Microbubble diameter at n% of the cumulative number ( $\mu m$ )
$D_p$	Pore diameter ( $\mu m$ )
$D_w$	Gas diffusivity in water ( $m^2.s^{-1}$ )
J	Phase flux of the gaseous phase ( $m^3.m^{-2}.s^{-1}$ )
L	Ostwald's coefficient
$n_i$	Number of microbubbles in the class i
$P_{atm}$	Atmospheric pressure (Pa)
$P^*$	Excess pressure (Pa)
$P_{PB}$	Bubble point pressure (Bar)
$\Delta P$	Transmembrane pressure (Bar)
$\delta P$	Laplace pressure (Pa)
Q	Volumic flowrate of the gaseous phase ( $m^3.s^{-1}$ )
r	Radius of the microbubble
R and $R_2$	Inner radius of the membrane tube (m)
$R_1$	Rod radius (m)
t	Time (s)
$V_d$	Mean velocity of the continuous phase in the tube ( $m.s^{-1}$ )

450

## Greek Symbols

$\gamma_0$	Surface tension at t=0 s ( $mN.m^{-1}$ )
$\gamma_{eq}$	Surface tension at the equilibrium ( $mN.m^{-1}$ )
$\mu$	Dynamic viscosity (Pa.s)
$\tau_w$	Shear stress at the membrane surface (Pa)
$\Theta$	Contact angle

## Abbreviations

$C_3F_8$	Octafluoropropane
CEHDA	Coaxial electrohydrodynamic atomisation
CMC	Critical micelle concentration
CV	Coefficient variation
PEG40S	Polyoxyethylene (40) stearate
PTFE	Polytetrafluorethylene
Tween20	Polyoxyethylene (20) sorbitan monolaurate
SDS	Sodium dodecyl sulfate
SPG	Shirasu Porous Glass

## 455 References

- [1] M. Kukizaki, T. Wada, Effect of the membrane wettability on the size and size distribution of microbubbles formed from Shirasu-porous-glass (SPG) membranes, *Colloids and Surfaces A: Physicochemical and Engineering Aspects* 317 (1-3) (2008) 146–154. doi:10.1016/j.colsurfa.2007.10.005.  
URL <http://linkinghub.elsevier.com/retrieve/pii/S0927775707009168>
- 460 [2] S. Khirani, P. Kunwapanitchakul, F. Augier, C. Guigui, P. Guiraud, G. Hébrard, Microbubble Generation through Porous Membrane under Aqueous or Organic Liquid Shear Flow, *Industrial & Engineering Chemistry Research* 51 (4) (2012) 1997–2009. doi:10.1021/ie200604g.  
URL <http://pubs.acs.org/doi/abs/10.1021/ie200604g>
- [3] C. Liu, T.-M. Xiao, J. Zhang, L. Zhang, J.-L. Yang, M. Zhang, Effect of membrane wettability on  
465 membrane fouling and chemical durability of SPG membranes used in a microbubble-aerated biofilm reactor, *Separation and Purification Technology* 127 (2014) 157–164. doi:10.1016/j.seppur.2014.03.001.  
URL <http://linkinghub.elsevier.com/retrieve/pii/S1383586614001439>
- [4] W. Krause (Ed.), *Optical, ultrasound, x-ray and radiopharmaceutical imaging*, no. 2.2002 in *Contrast*  
470 *agents*, Springer, Berlin, 2002, oCLC: 314296713.
- [5] K. Ferrara, R. Pollard, M. Borden, Ultrasound Microbubble Contrast Agents: Fundamentals and Application to Gene and Drug Delivery, *Annual Review of Biomedical Engineering* 9 (1) (2007) 415–447. doi:10.1146/annurev.bioeng.8.061505.095852.  
URL <http://www.annualreviews.org/doi/abs/10.1146/annurev.bioeng.8.061505.095852>
- 475 [6] S. Tinkov, R. Bekeredjian, G. Winter, C. Coester, Microbubbles as ultrasound triggered drug carriers, *Journal of Pharmaceutical Sciences* 98 (6) (2009) 1935–1961. doi:10.1002/jps.21571.  
URL <http://linkinghub.elsevier.com/retrieve/pii/S0022354916329835>

- [7] J. A. Feshitan, C. C. Chen, J. J. Kwan, M. A. Borden, Microbubble size isolation by differential centrifugation, *Journal of Colloid and Interface Science* 329 (2) (2009) 316–324. doi:10.1016/j.jcis.2008.09.066.  
480 URL <http://linkinghub.elsevier.com/retrieve/pii/S0021979708012149>
- [8] M. A. Parrales, J. M. Fernandez, M. Perez-Saborid, J. A. Kopechek, T. M. Porter, Acoustic characterization of monodisperse lipid-coated microbubbles: Relationship between size and shell viscoelastic properties, *The Journal of the Acoustical Society of America* 136 (3) (2014) 1077–1084. doi:10.1121/1.4890643.  
485 URL <http://asa.scitation.org/doi/10.1121/1.4890643>
- [9] Michel Schneider, BR1 : A new ultrasonographic contrast agent based on sulfur hexafluoride-filled microbubbles, *Investigate radiology*.
- [10] S. Rossi, C. Szjirt, F. Gerber, G. Waton, M. P. Krafft, Fluorous materials in microbubble engineering science and technology Design and development of new bubble preparation and sizing technologies, *Journal of Fluorine Chemistry* 132 (12) (2011) 1102–1109. doi:10.1016/j.jfluchem.2011.06.032.  
490 URL <http://linkinghub.elsevier.com/retrieve/pii/S002211391100220X>
- [11] M. P. Krafft, Fluorine in medical microbubbles Methodologies implemented for engineering and investigating fluorocarbon-based microbubbles, *Journal of Fluorine Chemistry* 177 (2015) 19–28. doi:10.1016/j.jfluchem.2015.02.013.  
495 URL <http://linkinghub.elsevier.com/retrieve/pii/S0022113915000585>
- [12] A. Kabalnov, D. Klein, T. Pelura, E. Schutt, J. Weers, Dissolution of multicomponent microbubbles in the bloodstream: 1. Theory, *Ultrasound in medicine & biology* 24 (5) (1998) 739–749.  
URL <http://www.sciencedirect.com/science/article/pii/S0301562998000349>
- [13] S. Rossi, G. Waton, M. P. Krafft, Small Phospholipid-Coated Gas Bubbles Can Last Longer than Larger Ones, *ChemPhysChem* 9 (14) (2008) 1982–1985. doi:10.1002/cphc.200800386.  
500 URL <http://doi.wiley.com/10.1002/cphc.200800386>
- [14] C. Szjirt, S. Rossi, G. Waton, M. P. Krafft, Effects of Perfluorocarbon Gases on the Size and Stability Characteristics of Phospholipid-Coated Microbubbles: Osmotic Effect versus Interfacial Film Stabilization, *Langmuir* 28 (2) (2012) 1182–1189. doi:10.1021/la2043944.  
505 URL <http://pubs.acs.org/doi/abs/10.1021/la2043944>
- [15] P. N. Nguyen, T. T. Trinh Dang, G. Waton, T. Vandamme, M. P. Krafft, A Nonpolar, Nonamphiphilic Molecule Can Accelerate Adsorption of Phospholipids and Lower Their Surface Tension at the Air/Water Interface, *ChemPhysChem* 12 (14) (2011) 2646–2652. doi:10.1002/cphc.201100425.  
510 URL <http://doi.wiley.com/10.1002/cphc.201100425>

- [16] S. R. Sirsi, M. A. Borden, Microbubble compositions, properties and biomedical applications, *Bubble Science, Engineering & Technology* 1 (1-2) (2009) 3–17. doi:10.1179/175889709X446507.  
URL <http://www.maneyonline.com/doi/abs/10.1179/175889709X446507>
- [17] V. Sanna, G. Pintus, P. Bandiera, R. Anedda, S. Punzoni, B. Sanna, V. Migaleddu, S. Uzzau, M. Sechi, Development of Polymeric Microbubbles Targeted to Prostate-Specific Membrane Antigen as Prototype of Novel Ultrasound Contrast Agents, *Molecular Pharmaceutics* 8 (3) (2011) 748–757. doi:10.1021/mp100360g.  
URL <http://pubs.acs.org/doi/abs/10.1021/mp100360g>
- [18] R. Shih, A. P. Lee, Post-Formation Shrinkage and Stabilization of Microfluidic Bubbles in Lipid Solution, *Langmuir* 32 (8) (2016) 1939–1946. doi:10.1021/acs.langmuir.5b03948.  
URL <http://pubs.acs.org/doi/10.1021/acs.langmuir.5b03948>
- [19] Z. Xing, H. Ke, J. Wang, B. Zhao, X. Yue, Z. Dai, J. Liu, Novel ultrasound contrast agent based on microbubbles generated from surfactant mixtures of Span 60 and polyoxyethylene 40 stearate, *Acta Biomaterialia* 6 (9) (2010) 3542–3549. doi:10.1016/j.actbio.2010.03.007.  
URL <http://linkinghub.elsevier.com/retrieve/pii/S1742706110001339>
- [20] Y. Ando, H. Tabata, M. Sanchez, A. Cagna, D. Koyama, M. P. Krafft, Microbubbles with a Self-Assembled Poloxamer Shell and a Fluorocarbon Inner Gas, *Langmuir* 32 (47) (2016) 12461–12467. doi:10.1021/acs.langmuir.6b01883.  
URL <http://pubs.acs.org/doi/abs/10.1021/acs.langmuir.6b01883>
- [21] E. Stride, M. Edirisinghe, Novel microbubble preparation technologies, *Soft Matter* 4 (12) (2008) 2350. doi:10.1039/b809517p.  
URL <http://xlink.rsc.org/?DOI=b809517p>
- [22] E. Stride, M. Edirisinghe, Novel preparation techniques for controlling microbubble uniformity: a comparison, *Medical & Biological Engineering & Computing* 47 (8) (2009) 883–892. doi:10.1007/s11517-009-0490-8.  
URL <http://link.springer.com/10.1007/s11517-009-0490-8>
- [23] R. Parmar, S. K. Majumder, Microbubble generation and microbubble-aided transport process intensification A state-of-the-art report, *Chemical Engineering and Processing: Process Intensification* 64 (2013) 79–97. doi:10.1016/j.cep.2012.12.002.  
URL <http://linkinghub.elsevier.com/retrieve/pii/S0255270112002292>
- [24] M. P. Krafft, Fluorine in medical microbubbles ? Methodologies implemented for engineering and investigating fluorocarbon-based microbubbles, *Journal of Fluorine Chemistry* 177 (2015) 19–28. doi:

10.1016/j.jfluchem.2015.02.013.

URL <http://linkinghub.elsevier.com/retrieve/pii/S0022113915000585>

- 545 [25] J.-M. Gorce, M. Arditì, M. Schneider, Influence of bubble size distribution on the echogenicity of ultrasound contrast agents: A study of SonoVue, *Investigative Radiology* 35 (11) (2000) 661–671.
- [26] A. M. Gan-Calvo, J. M. Gordillo, Perfectly Monodisperse Microbubbling by Capillary Flow Focusing, *Physical Review Letters* 87 (27). doi:10.1103/PhysRevLett.87.274501.  
URL <https://link.aps.org/doi/10.1103/PhysRevLett.87.274501>
- 550 [27] A. H. Dhanaliwala, A. J. Dixon, D. Lin, J. L. Chen, A. L. Klibanov, J. A. Hossack, In vivo imaging of microfluidic-produced microbubbles, *Biomedical Microdevices* 17 (1). doi:10.1007/s10544-014-9914-9.  
URL <http://link.springer.com/10.1007/s10544-014-9914-9>
- [28] Elena Castro-Hernandez, Wim van Hoeve, Detlef Lohse, Jose M. Gordillo, Microbubble generation in a  
555 co-flow device operated in a new regime, *Lab on a Chip* 11 (2011) 2023–2029. doi:10.1039/C0LC00731E.
- [29] J. H. Xu, S. W. Li, G. G. Chen, G. S. Luo, Formation of monodisperse microbubbles in a microfluidic device, *AIChE Journal* 52 (6) (2006) 2254–2259. doi:10.1002/aic.10824.  
URL <http://doi.wiley.com/10.1002/aic.10824>
- [30] M. Parhizkar, M. Edirisinghe, E. Stride, The effect of surfactant type and concentration on the size and  
560 stability of microbubbles produced in a capillary embedded T-junction device, *RSC Advances* 5 (14) (2015) 10751–10762. doi:10.1039/C4RA15167D.  
URL <http://xlink.rsc.org/?DOI=C4RA15167D>
- [31] U. Farook, E. Stride, M. Edirisinghe, Preparation of suspensions of phospholipid-coated microbubbles by  
565 coaxial electrohydrodynamic atomization, *Journal of The Royal Society Interface* 6 (32) (2009) 271–277.  
doi:10.1098/rsif.2008.0225.  
URL <http://rsif.royalsocietypublishing.org/cgi/doi/10.1098/rsif.2008.0225>
- [32] M. Kukizaki, M. Goto, Spontaneous formation behavior of uniform-sized microbubbles from Shirasu  
porous glass (SPG) membranes in the absence of water-phase flow, *Colloids and Surfaces A: Physico-  
chemical and Engineering Aspects* 296 (1-3) (2007) 174–181. doi:10.1016/j.colsurfa.2006.09.042.  
570 URL <http://linkinghub.elsevier.com/retrieve/pii/S092777570600731X>
- [33] M. Kukizaki, Microbubble formation using asymmetric Shirasu porous glass (SPG) membranes and  
porous ceramic membranes – A comparative study, *Colloids and Surfaces A: Physicochemical and  
Engineering Aspects* 340 (1-3) (2009) 20–32. doi:10.1016/j.colsurfa.2009.02.033.  
URL <http://linkinghub.elsevier.com/retrieve/pii/S0927775709001095>

- 575 [34] M. Kukizaki, M. Goto, Size control of nanobubbles generated from Shirasu-porous-glass (SPG) membranes, *Journal of Membrane Science* 281 (1-2) (2006) 386–396. doi:10.1016/j.memsci.2006.04.007.  
URL <http://linkinghub.elsevier.com/retrieve/pii/S0376738806002432>
- [35] M. Kukizaki, Y. Baba, Effect of surfactant type on microbubble formation behavior using Shirasu porous glass (SPG) membranes, *Colloids and Surfaces A: Physicochemical and Engineering Aspects* 326 (3)  
580 (2008) 129–137. doi:10.1016/j.colsurfa.2008.05.025.  
URL <http://www.sciencedirect.com/science/article/pii/S0927775708003452>
- [36] S. M. Joscelyne, G. Trägårdh, Membrane emulsification literature review, *Journal of Membrane Science* 169 (1) (2000) 107–117.  
URL <http://www.sciencedirect.com/science/article/pii/S0376738899003348>
- 585 [37] E. G. Schutt, D. H. Klein, R. M. Mattrey, J. G. Riess, Injectable Microbubbles as Contrast Agents for Diagnostic Ultrasound Imaging: The Key Role of Perfluorochemicals, *Angewandte Chemie International Edition* 42 (28) (2003) 3218–3235. doi:10.1002/anie.200200550.  
URL <http://onlinelibrary.wiley.com/doi/10.1002/anie.200200550/abstract>
- 590 [38] Q. Xu, M. Nakajima, S. Ichikawa, N. Nakamura, P. Roy, H. Okadome, T. Shiina, Effects of surfactant and electrolyte concentrations on bubble formation and stabilization, *Journal of Colloid and Interface Science* 332 (1) (2009) 208–214. doi:10.1016/j.jcis.2008.12.044.  
URL <http://linkinghub.elsevier.com/retrieve/pii/S0021979708016810>
- [39] M. S. Kalekar, S. S. Bhagwat, Dynamic Behavior of Surfactants in Solution, *Journal of Dispersion Science and Technology* 27 (7) (2006) 1027–1034. doi:10.1080/01932690600767080.  
595 URL <http://www.tandfonline.com/doi/abs/10.1080/01932690600767080>
- [40] T. Nakashima, M. Kawano, M. Shimizu, Articles of porous glass and process for preparing the same, US Patent No. 4,657,875, 1987.
- [41] G. T. Vladislavljević, Integrated membrane processes for the preparation of emulsions, particles  
600 and bubbles, in: *Integrated Membrane Systems and Process*, Wiley (2015) 79–140. doi:10.1002/9781118739167.ch5.
- [42] C. Charcosset, Membranes for the preparation of emulsions and particles, in: *Membrane Processes in Biotechnology and Pharmaceutics*, Elsevier, 2012, pp. 213–251. doi:10.1016/B978-0-444-56334-7.00006-X.  
605 URL <http://linkinghub.elsevier.com/retrieve/pii/B978044456334700006X>

- [43] H. S. Goran T. Vladislavljević, Preparation and analysis of oil-in-water emulsions with a narrow droplet size distribution using Shirasu-porous-glass (SPG) membranes, *Desalination* 144 (2002) 167–172. doi: 10.1016/S0011-9164(02)00307-7.
- [44] J. Benjamins, A. Cagna, E. H. Lucassen-Reynders, Viscoelastic properties of triacylglycerol/water inter-  
610 faces covered by proteins, *Colloids and Surfaces A: Physicochemical and Engineering Aspects* 114 (1996) 245–254. doi:10.1016/0927-7757(96)03533-9.
- [45] Talleyrand, *Fluides en écoulement méthodes et modèles - chapitre 6 Ecoulement Interne*, 1991.
- [46] B. E. Oeffinger, M. A. Wheatley, Development and characterization of a nano-scale contrast agent, *Ultrasonics* 42 (1-9) (2004) 343–347. doi:10.1016/j.ultras.2003.11.011.  
615 URL <http://linkinghub.elsevier.com/retrieve/pii/S0041624X03002117>
- [47] R. Liu, G. Ma, F.-T. Meng, Z.-G. Su, Preparation of uniform-sized PLA microcapsules by combining Shirasu Porous Glass membrane emulsification technique and multiple emulsion-solvent evaporation method, *Journal of Controlled Release* 103 (1) (2005) 31–43. doi:10.1016/j.jconrel.2004.11.025. URL <http://linkinghub.elsevier.com/retrieve/pii/S0168365904005863>
- 620 [48] M. Yasuno, S. Sugiura, S. Iwamoto, M. Nakajima, A. Shono, K. Satoh, Monodispersed microbubble formation using microchannel technique, *AIChE Journal* 50 (12) (2004) 3227–3233. doi:10.1002/aic.10276. URL <http://doi.wiley.com/10.1002/aic.10276>
- [49] G. Vladislavljević, M. Shimizu, T. Nakashima, Permeability of hydrophilic and hydrophobic Shirasu-  
625 porous-glass (SPG) membranes to pure liquids and its microstructure, *Journal of Membrane Science* 250 (1-2) (2005) 69–77. doi:10.1016/j.memsci.2004.10.017. URL <http://linkinghub.elsevier.com/retrieve/pii/S0376738804007112>
- [50] V. Schröder, O. Behrend, H. Schubert, Effect of dynamic interfacial tension on the emulsification process using microporous, ceramic membranes, *Journal of Colloid and Interface Science* 202 (2) (1998) 334–340.  
630 doi:10.1006/jcis.1998.5429.
- [51] M. Kukizaki, Shirasu porous glass (SPG) membrane emulsification in the absence of shear flow at the membrane surface: Influence of surfactant type and concentration, viscosities of dispersed and continuous phases, and transmembrane pressure, *Journal of Membrane Science* 327 (1-2) (2009) 234–243. doi:10.1016/j.memsci.2008.11.026.  
635 URL <http://linkinghub.elsevier.com/retrieve/pii/S0376738808009903>
- [52] m. Lepercq-Bost, M.-L. Giorgi, A. Isambert, C. Arnaud, Use of the capillary number for the prediction of droplet size in membrane emulsification, *Journal of Membrane Science* 314 (1-2) (2008) 76–89. doi:

10.1016/j.memsci.2008.01.023.

URL <http://linkinghub.elsevier.com/retrieve/pii/S0376738808000719>

- 640 [53] M. Yasuno, M. Nakajima, S. Iwamoto, T. Maruyama, S. Sugiura, I. Kobayashi, A. Shono, K. Satoh,  
Visualization and characterization of SPG membrane emulsification, *Journal of membrane science* 210 (1)  
(2002) 29–37.

URL <http://www.sciencedirect.com/science/article/pii/S037673880200371X>

- [54] J. J. Kwan, M. A. Borden, Microbubble Dissolution in a Multigas Environment, *Langmuir* 26 (9) (2010)  
645 6542–6548. doi:10.1021/la904088p.

URL <http://pubs.acs.org/doi/abs/10.1021/la904088p>

- [55] P. S. Epstein, M. S. Plesset, On the Stability of Gas Bubbles in LiquidGas Solutions, *The Journal of  
Chemical Physics* 18 (11) (1950) 1505–1509. doi:10.1063/1.1747520.

URL <http://aip.scitation.org/doi/10.1063/1.1747520>

- 650 [56] J. Hanwright, J. Zhou, G. M. Evans, K. P. Galvin, Influence of Surfactant on Gas Bubble Stability,  
*Langmuir* 21 (11) (2005) 4912–4920. doi:10.1021/la0502894.

URL <http://pubs.acs.org/doi/abs/10.1021/la0502894>